Thermochimica Acta, 203 (1992) 391–417
Elsevier Science Publishers B.V., Amsterdam

Kinetics of short-range ordering in αCu–Al alloys

Ari Varschavsky

Universidad de Chile, Facultad de Ciencias Físicas y Matemáticas,
Instituto de Investigaciones y Ensayes de Materiales, Casilla 1420, Santiago (Chile)

(Received 20 November 1991)

Abstract

The ordering behaviour in quenched αCu–Al was investigated by differential scanning calorimetry (DSC) under rising temperature conditions and by electron diffraction. It was found that the ordering processes can be better explained in terms of a homogeneous short-range order (SRO) model rather than a heterogeneous disperse order (DO) model as previously interpreted for the same type of experiments. The DSC traces indicate that the ordering takes place in two stages: the stage 1 ordering at lower temperatures is associated with the migration of excess vacancies and the stage 2 ordering at higher temperatures is associated with the migration of equilibrium vacancies. At higher temperatures, a marked surge of energy absorption occurs (stage 3) which is attributed to the destruction of order. For furnace-cooled alloys, only stage 3 appears. The relative dominance of stages 1 and 2 is influenced by the quenching temperature, the quench rate, the density of vacancy sinks and the sample shape before quenching. A relationship describing the overall SRO kinetics for both stages together, in terms of either the reacted fraction or the first SRO parameter, is proposed. A method for evaluating boundary values for this parameter is developed, making use of the features displayed by the DSC thermograms. The mobility of the vacancies, which controls their life-time and the short-range ordering rate, was evaluated by computing frequency factors and activation energies. Values for activation energies controlling the short-range ordering rate are somewhat smaller than the effective values obtained for stage 1 from the DSC traces, suggesting that the presence of solute–vacancy complexes may be important mainly as the aluminium concentration increases. From estimations of solute–vacancy and divacancy binding energies, it is inferred that divacancy formation is unlikely in the alloys under study. Process frequency factor values are in very good agreement with those calculated for a short-range order state developed during two-stage ordering by a vacancy mechanism. A flow diagram of the factors controlling the fractional increase of short-range order during anisothermal experiments is proposed.

INTRODUCTION

There has been continuing interest in the local-order structure of the α-phase in Cu–Al alloys since the electrical resistivity studies on neutron-

Correspondence to: A. Varschavsky, Universidad de Chile, Facultad de Ciencias Físicas y Matemáticas, Instituto de Investigaciones y Ensayes de Materiales, Casilla 1420, Santiago, Chile.

Dedicated to Professor Joseph H. Flynn in honour of his 70th birthday

irradiated material by Wechsler and Kernohan [1] indicated that a composition-dependent, diffusion-controlled, solid-state reaction occurs under certain conditions. Perhaps the most comprehensive study of such reactions in this system is that of Matsuo and Clarebrough [2] who identified the presence of short-range order (SRO) by calorimetry and resistivity measurements suggesting the role of vacancies in the kinetics of ordering. Further evidence of SRO in αCu–Al alloys has been reported by Borie and Sparks [3] using diffuse X-ray scattering and by Panin et al. [4] using density and resistivity measurements. In the literature cited above, it is clear that SRO in αCu–Al has been well identified.

The different features of ordering have been investigated, for instance, by diffuse scattering of X-rays [3,5–9], by small-angle X-ray scattering [10], by electron microscopy and electron diffraction [11–15], by determination of elastic and plastic properties [16–18], and strengthening and fatigue properties [19–24], as well as by electrical resistivity [25–28] and thermal analysis [16,17,21,29–34]. Two of these studies [14,16] inferred that after isothermal annealing at a temperature of 523 K (which is around the estimated critical value for domain dissolution [34]), for 1800 s, a disperse order (DO) state could be detected in quenched Cu–19 at.% Al. These findings were fairly consistent with the measured diffusion time (2400 s) at 518 K for furnace-cooled alloys pre-annealed for 80 h, where no excess vacancies were available [34]. However, for the same alloy, analysis of data obtained from non-isothermal experiments at different heating rates employing differential scanning calorimetry (DSC) [32], confirmed that the relaxation times at peak temperatures were about three orders of magnitude less than the calculated diffusion times required for an equilibrium DO state to be developed at those temperatures [14,16]. At lower aluminium concentrations, such differences become even larger [34]. Furthermore, the critical temperature for domain dissolution, which occurs by a first-order transition [34], is lower than the temperatures at which the ordering process goes to completion for the range of heating rates usually employed in DSC scans [2,16,32]. Thus, it seems unlikely that ordered regions would develop in quenched alloys during rising temperature experiments where ordering reactions have to take place before disordering commences.

Therefore, one sees that while this alloy system has been rather intensively investigated for a long time, no fully acceptable description of the kind of local order has evolved, the interpretation of the results being strongly influenced by the type of experiments carried out. In addition, although the study of short-range ordering phenomena in αCu–Al alloys continues [35,36], there is comparatively little research concerning the kinetics of the SRO process from a quantitative treatment of DSC traces. This technique is particularly appropriate if a statistical SRO model is suitable, because for these alloys, the changes in internal energy can be

represented effectively by the change in the order parameter for the first coordination shell as it was demonstrated by Kuwano et al. [37].

The principal objectives of the present work are: to determine whether during non-isothermal experiments performed in quenched and furnace-cooled alloys a homogeneous rather than a heterogeneous SRO state is developed; to propose relationships describing the overall SRO kinetics by means of DSC techniques; to compute boundary values for the first SRO parameter from the features displayed by the DSC traces (thus enabling the capabilities of the technique to be enhanced); to investigate the relative dominance of the stages involved in the ordering process after different quenching conditions in an attempt to clarify the effect of excess vacancies; and to determine the vacancy behaviour during the return of SRO to equilibrium.

MATERIAL AND EXPERIMENTAL METHOD

The three αCu–Al alloys studied contained, respectively, 3.00 ± 0.04, 6.00 ± 0.07 and 9.0 ± 0.10 wt.% aluminium (99.97 wt.%). They were prepared in a Baltzer VSG 10 vacuum induction furnace from electrolytic copper (99.95 wt.%) in a graphite crucible. The ingots were subsequently forged at 923 K to a thickness of 10 mm, pickled with a solution of nitric acid (15% in distilled water) to remove surface oxide, annealed in a vacuum furnace at 1123 K for 36 h to achieve complete homogeneity, and cooled in the furnace to room temperature. They were cold-rolled to 1.5 mm thickness with intermediate annealing periods at 923 K for one hour. After the last anneal, the material was finally rolled to 0.75 mm thickness (50% reduction). A subsequent heat treatment was performed at 873 K for one hour, followed by quenching. Microcalorimetric analysis of the samples was performed in a Du Pont 2000 thermal analyser. Specimen discs of 0.75 mm thickness and 6 mm diameter were prepared and examined for each material condition. Differential scanning calorimetric measurements of the heat flow were made by operating the calorimeter in the constant heating mode (heating rates of 0.83, 0.33, 0.17, 0.083 and 0.033 K s^{-1}). Runs were made from room temperature to 740 K. To increase the sensitivity of the measurements, a high purity, well-annealed copper disc, in which no thermal events occur over the range of temperatures scanned, was used as a reference. In order to minimize oxidation, dried nitrogen (0.8×10^{-4} m^3 min^{-1}) was passed through the calorimeter.

Thin foils suitable for transmission electron microscopy were prepared by cutting sheets in a Servomet spark-cutter machine. The sheets were electrolytically thinned to a thickness of 0.06 mm using a 50% phosphoric acid and 50% ethyl alcohol solution. Then discs were shaped from the sheets in the spark-cutter machine, using a special holder developed in our laboratory. Some discs were quenched from 873 K, introduced in the

calorimeter and heated at a heating rate of 0.033 K s^{-1} up to 515 K, followed by quenching. Some other discs were quenched from 873 K and annealed for 1 h at 515 K, and finally another batch of discs were simply quenched from the same temperature. Then, all discs were subjected to a final electrolytic thinning in a Struers Tenupol machine using the same solution as above. Electron diffraction was performed in a Philips EM-300 electron microscope.

RESULTS AND DISCUSSION

DSC thermograms for quenched alloys

Typical thermograms for the three alloys are shown in the differential heat capacity ΔC_p versus temperature (T) curves at the indicated heating rates ϕ in Fig. 1. They are characterized by two exothermic peaks, namely stages 1 and 2 and one endothermic peak, stage 3. Stages 1 and 2 have been reported in the literature in connection with short-range order development assisted by the migration of excess vacancies and by the migration of equilibrium vacancies respectively, while stage 3 has been associated with a disordering process [2,17,38]. The height and area under all of these peaks increase with the aluminium content.

It can be observed in Fig. 1 that all stages shift to lower temperatures as the aluminium concentration $\bar{c}$ increases. Also the relative dominance of

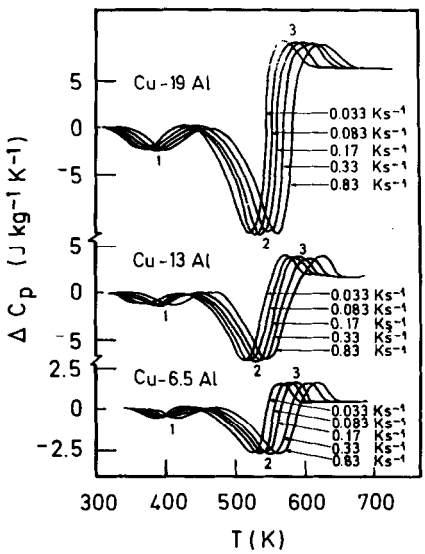

Fig. 1. DSC thermograms for αCu–Al alloys quenched from 873 K. Each curve is labelled with the heating rate.

the different stages is independent of the heating rate. These features reflect that all reactions are kinetically controlled. A kinetically controlled dissolution process is expected from a homogeneous SRO state or from the dissolution of particles taking place by a second-order transition [39]. However in the latter case, the width and height of stage 3 are dependent on the heating rate [39]. If the dissolution occurs by a first-order transition as in a DO state in αCu–Al alloys, where ordered domains are based on the Cu_3Al structure [11,14], the process is thermodynamically controlled and, hence, the peak temperature of stage 3 is independent of the heating rate. However, none of these features are observed in Fig. 1; the latter behaviour has been reported during non-isothermal scans for two-stage ordering in alloys exhibiting heterogeneous order [40–42]. Therefore, the observed heating rate dependence of the peak temperature of stage 3 and its associated shape invariability reflects the disordering of a homogeneous SRO state. Regarding the effect of Al content on the temperature at which the maximum of stage 3 takes place for a given heating rate, it can be seen in Fig. 1 that this temperature is independent of the alloy composition. This can also be interpreted in terms of the disordering of a homogeneous SRO state. In fact, if this stage is attributed to the dissolution of disperse ordered domains, a shift to lower temperatures with decreasing aluminium content would be expected, because finer particles are predicted to be developed according to Aubauer's model of DO [43]. Finer particles reduce the dissolution temperature because of the increased surface-to-volume ratio. Hence, from the features displayed in the DSC traces for the present quenching conditions it is expected that a homogeneous SRO state develops in two stages. However, additional evidence is necessary to confirm this; this is presented in the following two sections.

The areas under the ΔC_p versus T curves which correspond to the enthalpies of the different reactions in stages 1, 2 and 3 are listed in Table 1. The enthalpy absorption associated with stage 3 was evaluated by considering the area of the ΔC_p versus T curve between the temperature at which the curve of stage 2 crosses the baseline and the temperature at which energy is absorbed at a constant rate from the baseline. The enthalpy of exotherms 1 and 2 was determined by integrating the area below the maximum in the DSC scan. As expected, it can be noticed that

TABLE 1

Enthalpimetric data for stages 1, 2 and 3 measured at $\phi = 0.33$ K s^{-1}

Material (at.% Al)	$-\Delta H_1$ (J mol^{-1})	$-\Delta H_2$ (J mol^{-1})	ΔH_3 (J mol^{-1})
19	11.3	28.3	25.8
13	6.9	18.9	15.5
6.5	2.3	8.9	5.0

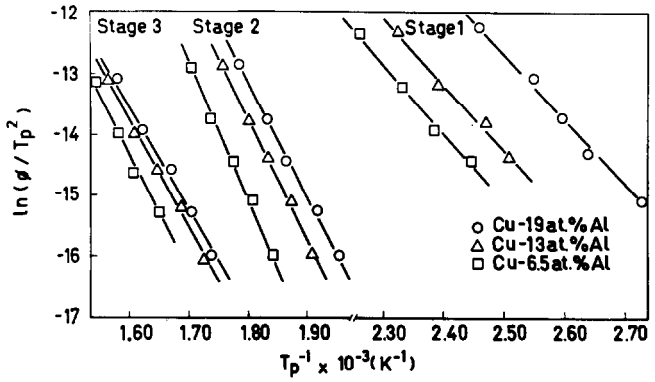

Fig. 2. Kissinger plots for αCu–Al alloys quenched from 873 K.

all of these enthalpies increase as the alloy becomes more concentrated. It was also verified that their values are independent of the heating rate. In order to have a deeper insight into all these processes, a kinetic study was performed, see below. Values appearing in Table 1 for stages 1 and 2 are used later in connection with this analysis.

Kinetic parameters and kinetic laws

Values for the activation energies are required to perform the non-isothermal kinetic analysis. These values were computed using Kissinger's peak-shift method [44]. Figure 2 shows the dependence of $\ln(\phi/T_p)$ on $1/T_p$ for the three stages, where T_p is the peak temperature. The corresponding lines, with slopes $-E/R$, give an evaluation of the activation energy E for each process; these values are listed in Table 2.

It can be seen from Table 2 that the activation energies for stage 1, although somewhat higher, are consistent with those for vacancy migration [45], while those for stage 2 agree reasonably well with those for self-diffusion reported in the literature [25,28,46]. These values decrease with aluminium content, which is consistent with the decrease in atomic mobility usually found in solid solutions of copper as the solute concentration

TABLE 2

Activation energies for the three stages observed in quenched αCu–Al alloys

Material (at.% Al)	E_1 (kJ mol^{-1})	E_2 (kJ mol^{-1})	E_3 (kJ mol^{-1})
19	87.7	148.6	150.1
13	89.6	161.9	159.8
6.5	93.5	180.3	179.1

decreases [47]. The above tendency for both activation energies is also consistent with the observed increase in the peak temperatures of stages 1 and 2, as the alloys become less concentrated. It can also be noticed that the activation energies for disordering are practically the same as those computed for stage 2. This is inconsistent with a diffusion-controlled nucleation and growth of ordered particles in a disordered matrix. If this is so, then ordering rates slower than disordering rates would be expected, which is not the case in the present work, as calculated below.

The next step is to assign a suitable law to the experimental reacted fractions y_1, y_2 and y_3 for stages 1, 2 and 3 respectively. A non-invoking mechanism method will be assumed [48]. The integrated kinetic approach under non-isothermal conditions gives

$$\frac{1-(1-y)^{1-n}}{1-n} = k_0\theta \tag{1}$$

where n is the order of reaction designated as the order parameter for solid-state reactions, k_0 is the process frequency factor (also termed the pre-exponential factor) and θ is the reduced time (the time at which the reaction goes to completion at an infinite temperature). Its value can be calculated from [49]

$$\theta = \frac{RT^2}{\phi E}\exp\left(-\frac{E}{RT}\right) \tag{2}$$

where T is the temperature and R the universal gas constant.

For the correct value of n, a plot of $(1-(1-y)^{-1})/(1-n)$ against θ will give a straight line of slope k_0. Equation (1) applies for all values of n, except $n = 1$, for which the equation is

$$\ln\left(\frac{1}{1-y}\right) = k_0\theta \tag{3}$$

Equation (1) was tested with the present data with unsuccessful results. However, it was possible to compute process frequency factors from plots of $\ln(1/(1-y))$ versus θ. These plots, which resulted in straight lines of slope k_0, are shown in Fig. 3, thus confirming that a first-order kinetic law can be associated with all the stages. The applicability of a specific phenomenological model to a certain solid-state reaction has been discussed extensively [50–52].

From the values of E_2 and k_{02}, the relaxation times at peak temperatures T_{p2} of stage 2 extrapolated to $\phi = 0$ (500, 505 and 510 K for 19, 13 and 6.5% Al), $\tau_2 = k_{02}^{-1}\exp(E_2/RT_{p2})$, can be calculated and compared with the diffusion times $t_{0.5}$ required for an equilibrium DO ordered state to be attained. One obtains $\tau_2 = 19$, 93 and 836 s for 19, 13 and 6.5% Al, these being the upper limiting values. However, $t_{0.5} = 4.3 \times 10^4$, 22.3×10^4

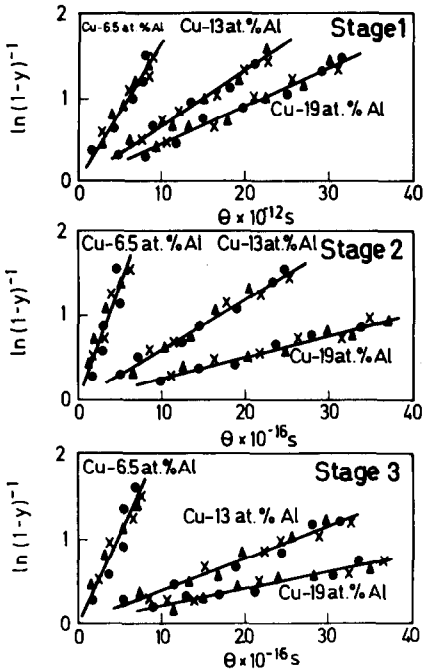

Fig. 3. Plots of $\ln[(1-y)^{-1}]$ vs. θ for αCu–Al alloys quenched from 873 K; $\phi = 0.33$ K s^{-1}.

and 5400×10^4 s [34] for 19, 13 and 6.5% Al at the same temperatures. For Cu–19% Al, the relaxation time is almost three orders of magnitude lower than the diffusion time, this difference being more important as the Al concentration decreases. However, the relaxation times at peak temperatures T_{p3} of stage 3 extrapolated to $\phi = 0$ (545, 548, 550 K for 19, 13, 6.5% Al), $\tau_3 = k_{03}^{-1} \exp(E_3/RT_{p3})$, are 1.2, 4.5 and 39.3 s for 19, 13 and 6.5% Al. These results indicate that the ordering rates are effectively lower than the disordering rates, which as already pointed out, is inconsistent with a diffusion-controlled nucleation and growth of ordered particles.

TABLE 3

Values of process frequency factors for the three stages observed in quenched αCu–Al alloys

Material (at.% Al)	k_{01} ($\times 10^{10}$ s^{-1})	k_{02} ($\times 10^{14}$ s^{-1})	k_{03} ($\times 10^{14}$ s^{-1})
19	4.6	2.6	2.0
13	6.7	6.0	3.8
6.5	17.0	35	26

Electron diffraction

Electron diffraction patterns in Cu–19% Al were recorded in the electron microscope. The spot patterns have limitations derived mainly from the fact that extension of reciprocal lattice points into relroads can lead to the possibility of reflections over a large angular range. To avoid this complication, the diffraction patterns were taken with the foil tilted in an exact orientation. Figure 4(a) shows a selected area diffraction pattern of a quenched disc specimen from 873 K. Only matrix reflections are observed and diffuse scattering is absent, indicating that the alloy is in an almost disordered state. Figure 4(b) shows a selected area diffraction pattern of a disc specimen quenched from 873 K and annealed at 515 K for 1 h; here well-defined superlattice reflections with a distribution of the reflection points typical of a periodic anti-phase structure can be observed. It is evident that a disperse ordering process has taken place [14,16]. However, when a disc specimen quenched from the same temperature is heated in the calorimeter at a heating rate of 0.033 K s^{-1} up to 515 K (the peak temperature for stage 2), followed by quenching, only diffuse scattering is observed as illustrated in the diffraction pattern of Fig. 4(c). The extra spots appearing in Fig. 4(b) are not well defined when the alloy is in the above condition. The diffraction pattern of Fig. 4(c) is indicative of the presence of SRO intensity fluctuations; the four maxima in the diffuse scattering at the 110 positions in the reciprocal space are intersections of diffuse streaks [14]. Also, there are superimposed reflections belonging to segments of some rings for Cu_2O, possibly due to a surface layer. The low heating rate employed in heating this specimen was chosen in order to increase the time range from the initial temperature of stage 1 to the peak temperature of stage 2.

Overall kinetics for stages 1 and 2

Having confirmed that stages 1 and 2 correspond to the return of SRO to equilibrium via two processes, each obeying a first-order kinetic law, it

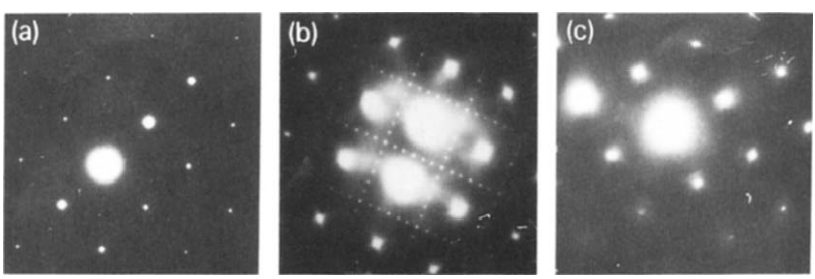

Fig. 4. Diffraction patterns in the [001] zone of Cu–19 at.% Al after different heat treatments (see text).

will now be demonstrated that they can be depicted by a single relationship. This expression can be written as a convex linear combination

$$y = \psi y_1 + (1 - \psi) y_2 \tag{4}$$

where

$$y_1 = 1 - \exp(-k_{01}\theta_1) \tag{5}$$

$$y_2 = 1 - \exp(-k_{02}\theta_2) \tag{6}$$

θ_1 and θ_2 being the θ function when E_1 or E_2 are used respectively and $\psi = \Delta H_1/(\Delta H_1 + \Delta H_2)$. It should be noted that ψ is a measure of the excess vacancy mechanism contribution to the return of SRO. Thus, if $\psi = 1$, equilibrium SRO order is attained via an excess vacancy mechanism only; $\psi = 0$ indicates that ordering takes place assisted exclusively by equilibrium vacancies. Certainly, under the quenching conditions imposed on the samples used in the present work, both mechanisms are contributing to complete the ordering process. Moreover, in αCu–Al alloys the change in internal energy can be described entirely by the first SRO parameter [37]. This is also supported by the fact that both ordering processes obey a first-order kinetic law [53,54]. Hence, the transformed fraction for both stages can be expressed as

$$y = \frac{\alpha - \alpha_{E_1}}{\alpha_{T_3} - \alpha_{E_1}} \tag{7}$$

and, therefore, eqn. (4) yields

$$\alpha = \alpha_{E_1} + (\alpha_{T_3} - \alpha_{E_1})\{\psi[1 - \exp(-k_{01}\theta_1)] + (1 - \psi)[1 - \exp(-k_{02}\theta_2)]\} \tag{8}$$

where α_{T_3} is the equilibrium first SRO parameter when stage 2 goes to completion, and α_{E_1} is the value retained after quenching. The temperature dependence of α is mostly independent of the SRO model chosen (quasi-chemical theory in pair approximation, cluster variation method, etc. [54]). We will adopt an equilibrium Warren–Cowley parameter

$$\alpha = 1 - \frac{p^{e}_{Cu-Al}}{\bar{c}} \tag{9}$$

where p^{e}_{Cu-Al} is the conditional probability of finding an aluminium atom next to a given Cu atom, $\bar{c}$ is the aluminium concentration as defined earlier, and the superscript e denotes the equilibrium value. The conditional probability can be calculated from [55]

$$p^{e}_{Cu-Al} = \frac{-1 + \{[1 + 4(1 - \bar{c})\bar{c}(w^2 - 1)]\}^{1/2}}{2(1 - \bar{c})(w^2 - 1)} \tag{10}$$

where $w^2 = \exp(2W/RT)$, $W = V_{Cu-Al} - 0.5(V_{Cu-Cu} + V_{Al-Al})$ is the ordering energy and V_{ij} is the binding energy of a Cu–Al atomic pair.

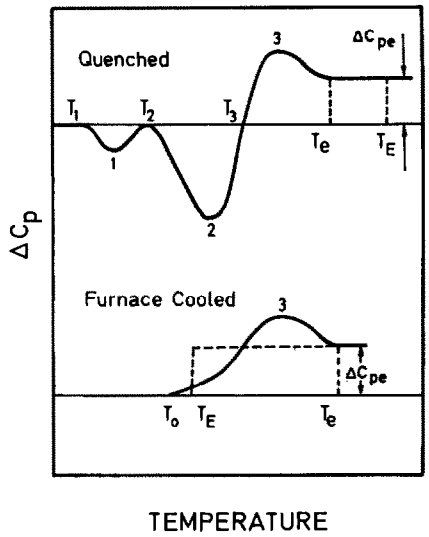

Fig. 5. DSC thermogram showing a schematic representation of a two-stage ordering process followed by a disordering stage in a quenched alloy. T_{E_1} may be simply specified as the temperature at which the equilibrium degree of order corresponding to that temperature is obtained at room temperature; and DSC trace for a disordering process in a furnace-cooled alloy.

Boundary values for α_{E_1} can be estimated as follows. Because energy evolutions during non-isothermal scans are due to the return of SRO ordering and energy absorptions are due to its destruction, then the degrees of order present at room temperature after quenching may be specified in terms of an equivalent temperature T_{E_1} at which these degrees of order would be in equilibrium [21]. In order to make the method straightforward, a schematic representation of a DSC trace for a two-stage ordering process followed by disordering, is shown in Fig. 5. Also, a DSC trace for a disordering process in a furnace-cooled alloy is shown here. From Fig. 5, for a given quenching temperature, T_{E_1} can be calculated from a knowledge of the net absorption or evolution of energy up to some temperature at which a constant rate of destruction of order has been attained, and the rate of absorption of energy on continuous heating above such temperature. If $\Delta H_1(T_1, T_2)$, $\Delta H_2(T_2, T_3)$, $\Delta H_3(T_3, T_e)$ are the energies associated with the respective peaks, and $\Delta H_{E_1} = \Delta C_{pe}(T_{E_1} - T_e)$ where ΔC_{pe} and T_e represent the constant differential specific heat and equilibrium temperature at which energy commences to be absorbed at a constant rate, then $\Delta H_{E_1} = \Delta H_1(T_1, T_2) + \Delta H_2(T_2, T_3) - \Delta H_3(T_3, T_e)$. Therefore, T_{E_1} can be determined from

$$T_{E_1} = T_e + \frac{\Delta H_1(T_1, T_2) + \Delta H_2(T_2, T_3) - \Delta H_3(T_3, T_e)}{\Delta C_{pe}} \tag{11}$$

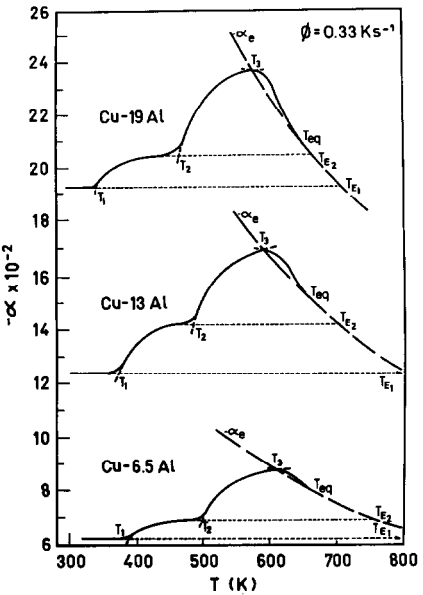

Fig. 6. Variation of the first SRO parameter for αCu–Al alloys quenched from 873 K. The α_e curves represent the equilibrium first SRO parameter as a function of temperature.

Substituting T_{E_1} in the expression for w^2 and using eqns. (10) and (9), α_{E_1} can be computed for each alloy composition. The ordering energy for αCu–Al alloys was taken as $W = -3.66$ kJ mol^{-1} [12,56]. Figure 6 shows the evolution of the first SRO parameter for the three alloys under study calculated from eqn. (8) from room temperature to T_3. Also its variation from T_3 to T_e was calculated separately by employing an expression for $y_3 = ((\alpha - \alpha_e)/(\alpha_3 - \alpha_e))$, similar to eqns. (5) and (6) but using k_{03} and θ_3 based on the values of E_3. α_e curves were also drawn in the same figure using eqns. (9) and (10). It can be noticed that after the first process was completed at T_2, an equilibrium degree of short-range order corresponding to T_{E_2} was reached. Because this increase in α between T_1 and T_2 is assisted by excess vacancies, the equivalent equilibrium SRO parameter at T_2, α_{E_2}, corresponds to the equilibrium degree attained after all excess vacancies have been annihilated on sinks. (Vacancy migration toward sinks assists the rearrangement of atoms for ordering.) As the temperature is increased, the equilibrium value of α at T_3 via an equilibrium vacancy-assisted ordering mechanism is reached, that is when vacancies form and are annihilated at the same rate. Calculated values for α_{E_2} from

$$T_{E_2} = T_e + \frac{\Delta H_2(T_2, T_3) - \Delta H_3(T_3, T_e)}{\Delta C_{pe}} \tag{12}$$

in conjunction with eqns. (10) and (9) are in excellent agreement with

values measured at T_2 in Fig. 6. This fact reflects that the procedure employed to evaluate boundary values for equivalent equilibrium SRO parameters at the beginning of a particular stage are quite adequate. In Fig. 6, the α kinetic paths between T_3 and T_e surpass the α curves because during the destruction of SRO order on continuous heating, the alloys fail to attain a permanent equilibrium state merely from the kinetically controlled nature of the reaction.

Furnace-cooled alloys

For the furnace-cooled alloys, a single disordering stage 3 is observed [21,28] which is shown schematically in Fig. 5(b). In this situation

$$T_E = T_e - \frac{[\Delta H_3(T_0, T_e)]}{\Delta C_{pe}} \tag{13}$$

where T_0 is the initial temperature in the absence of quenched-in vacancies (cooling rate, 15 K h^{-1}). Thus, α can be obtained from eqns. (9), (10) and (13), using equations of the type of eqns. (3) and (7). Hence

$$\alpha = \alpha_e - (\alpha_e - \alpha_E) \exp(-k_0\theta) \tag{14}$$

between T_0 and T_e, where k_0 is the corresponding pre-exponential factor. The pertinent thermograms are shown in Fig. 7 at the indicated heating rates. As pointed out before, the single stage 3 appearing there is representative of a disordering process. There are considerable shifts in the maxima

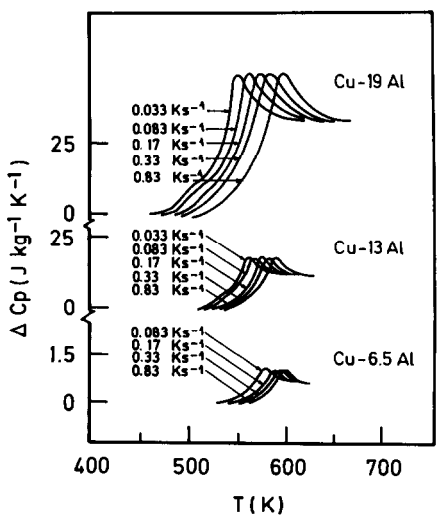

Fig. 7. DSC thermograms for αCu–Al alloys furnace-cooled at 15 K h^{-1}. Each curve is labelled with the heating rate.

TABLE 4

Values of activation energies and pre-exponential factors for furnace-cooled alloys at 15 K h^{-1}

	Cu–19% Al	Cu–13% Al	Cu–6.5% Al
E (J mol^{-1})	156 $\times 10^3$	151 $\times 10^3$	171 $\times 10^3$
k_0 (s^{-1})	1.4×10^{14}	4.2×10^{14}	25.0×10^{14}

of the rate of transformation curves to higher temperatures with increasing heating rate, implying again that this process is kinetically controlled. From such traces, boundary values for the short-range order parameter can be evaluated employing eqns. (9), (10) and (13), as for the quenched alloys. Activation energies and also k_0 values were computed as before. These value are listed in Table 4.

From the above data, the variation of α with temperature is plotted in Fig. 8. The path of the kinetic curves for α are higher than those corresponding to equilibrium because during the destruction of order on continuous heating, the alloys fail to attain a permanent equilibrium degree of order until $T = T_c$. This feature means that the alloys are in a state of order higher than that of equilibrium. Furthermore, the kinetic and equilibrium curves intercept each other at temperatures slightly higher than T_E

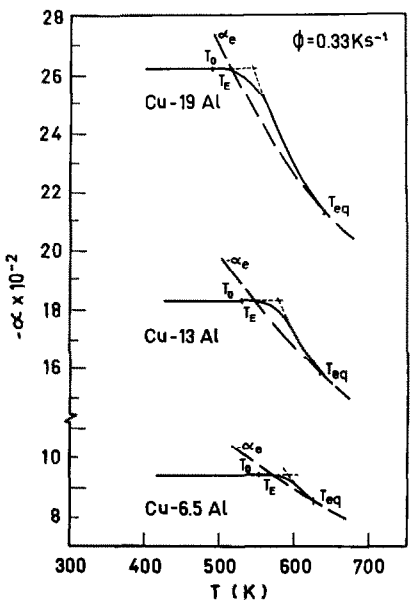

Fig. 8. Variation of the SRO parameter in furnace-cooled αCu–Al alloys (cooling rate 15 K h^{-1}). The α_e curves represent equilibrium values of the short-range order parameter as a function of temperature.

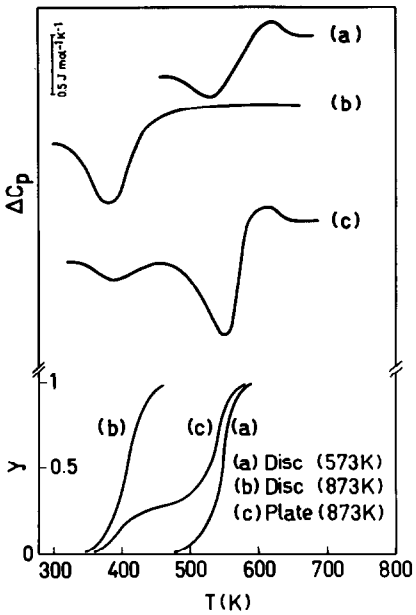

Fig. 9. DSC thermograms for Cu–19 at.% Al under different quenching conditions (upper curves) and the corresponding reacted fractions y (lower curves). The quenching temperatures are indicated. Both discs were quenched using a high-quenching-rate device; $\phi = 0.33$ K s^{-1} (see text).

in all cases, which can be naturally attributed to the expected behaviour of eqn. (14) between T_0 and T_e.

Effect of quenching conditions

From eqns. (4)–(6), the transformed fraction for the SRO reaction via both non-overlapping processes can be also expressed as

$$y = \psi[1 - \exp(-k_{01}\theta_1)] + (1 - \psi)[1 - \exp(-k_{02}\theta_2)] \quad (15)$$

As pointed out before, ψ is a measure of the dominance of stage 1, which is, in turn, determined by the quenching conditions, namely quenching temperature, quenching rate and specimen shape. Disc-shaped samples of Cu–19% Al quenched from two different temperatures using a high quenching rate device ($\approx 2 \times 10^4$ K s^{-1}) were supplied to us. The upper part of Fig. 9 shows DSC traces at $\phi = 0.33$ K s^{-1} under different quenching conditions. Curve (a) is the result of such a disc sample quenched from 573 K. It can be seen that $\psi = 0$. In this case equilibrium is reached via an equilibrium vacancy mechanism only. Curve (b) corresponds to one of these disc specimens quenched from 873 K. There is only a single peak corresponding to stage 1 SRO ordering and $\psi = 1$. This behaviour is

observed because the quenching rate is high and also because the specimen surface-to-volume ratio (disc) is large. Curve (c) corresponds to sample quenched from 873 K under normal conditions that have a plate shape before quenching, which is the case in the present experiments. Although for this sample the quenching temperature is the same as for the disc, the quenching rate is slower and fewer vacancies are frozen in. As a result, insufficient excess vacancies remain to complete SRO through stage 1.

The lower part of Fig. 9 shows the corresponding y against T kinetic curves. It can be seen, consistently with the thermograms, that equilibrium SRO is attained at lower temperatures when only stage 1 is present. In the kinetic path for curve (c), both stages are apparent. Curve (a) only exhibits stage 2, the ordering process being completed at a higher temperature (the equilibrium first SRO parameter is smaller). The kinetic parameters for curves (a) and (b), determined in the same manner as for curve (c), are $E = 146$ and 88 kJ mol^{-1}, and $k_0 = 2.8 \times 10^{14}$ and 7.2×10^{10} s^{-1}, also obeying a first-order kinetic law. These results are not shown here, for brevity.

Vacancy behaviour

Bounded vacancies

Solute–vacancy binding in αCu–Al alloy may be important regarding the effective vacancy mobility. In general, the binding effect arises from two factors, namely the size factor and the electronic factor [57]. The size factor is responsible for the strain field being produced by the size mismatch for oversized solute elements such that the lattice strain so produced is minimized by a vacancy–solute atom association. The electronic factor, however, is considered to be prevalent in the presence of a solute element of valency higher than that of the host element. In the case of αCu–Al alloys, both factors are present. Hence, a non-negligible binding energy is expected between an Al–vacancy complex. If it is considered that the values for E_1 are the effective activation energies for vacancy migration and those for E_2 the activation energies for interdiffusion, the effective formation energy of a vacancy is $E_f = E_2 - E_1$. These values are 60.7, 72.3 and 86.8 kJ mol^{-1} for 19, 13 and 6.5% Al. Because all expressions relating the effective vacancy formation energy to the solute–vacancy binding energy E_{vs} are valid only for dilute alloys, interpolated values for E_f are required. For 3.5 and 1.0 at.% Al, one obtains 94.5 and 101.2 kJ mol^{-1} respectively, taking for pure copper $E_v^f = 106.4$ kJ mol^{-1} [58]. The interpolated values for E_f were substituted into eqn. (16) [59]

$$E_f = E_v^f - E_{vs}\left[\left(\frac{1-12\bar{c}}{12\bar{c}}\right)\exp\left(-\frac{E_{vs}}{RT_q}\right)+1\right]^{-1} \tag{16}$$

It can be seen that E_f is not a linear function of T_q. However, it is found experimentally through measurements of the excess resistivity introduced by quenching $\Delta\rho_a$ that for varying quench temperatures over a sufficiently narrow range of values of T_q, $d \ln \Delta\rho_a/d(1/T_q) \simeq -E_f/R$. Iterative calculated values of E_{vs} for 3.5 and 1.0 at.% Al alloys quenched from 873 K give 23.2 and 20.3 kJ mol^{-1}. No literature data are available for comparison purposes, to the best of our knowledge. An average value of $E_{vs} = 21.8$ kJ mol^{-1} (0.21 eV) was obtained. Such a value is considered high enough in that an important fraction of atoms might be bounded [60]. These less mobile complexes increase the effective activation energy for vacancy migration E_1 as compared with the reported values for the activation energies of migration of mono-vacancies in the case of quenching from moderate temperatures [61]. However, the existence of such complexes should reduce the effective activation energy for vacancy formation. It is then expected that both effects become more pronounced as the ratio of bounded to total number of vacancies increases, which occurs (at a given temperature) as the alloy becomes more concentrated [62,63]. Hence, although values for activation energies for vacancy migration and formation decrease with increasing aluminium content as a consequence of the increasing atomic mobility [42], the measured values for $(E_2 - E_1)/E_1$ should decrease. In fact, such values are 0.69, 0.80 and 0.93 for 19, 13 and 6.5% Al. (Disintegration of solute–vacancy complexes can also take place during stage 2 ordering, as inferred later on [64].) It is interesting to point out also that $E_{vs} + E'_{vs} = 2W$ [62], E'_{vs} being the Cu–vacancy binding energy which amounts to -29.1 kJ mol^{-1}, indicating a strong repulsion.

In order for the trapping rate of vacancies by solute atoms to be important with respect to the thermal release in determining the bounded vacancy concentration, $E_{vs} \geq 5RT$ [65], which in the present case gives $T \leq 524$ K. This means that the trapping effect is more dominant in stage 1 than in stage 2. Hence, during this stage transport by the association–dissociation reaction and by migration of complexes is also to be expected.

Another effect connected with vacancy behaviour, which influences the effective activation energy for migration and hence the ordering rate, will be considered below.

Vacancy mobility

The relation between the vacancy jump frequency and the ordering rate will now be considered. The mobility of vacancies influences the ordering rate in two ways. Firstly, it controls the lifetime of vacancies and, hence, their concentration. In this respect, although the vacancy interchanges alternately with atoms on either of the constituent elements, Cu and Al, the two types of jumps cannot be distinguished in the definition of the average migration rate of vacancies to sinks and the associated lifetime.

The vacancy mobility ν_m is simply the sum of its interchange frequencies with atoms of Cu and Al. Hence

$$\nu_m = \nu_{Cu} + \nu_{Al} \tag{17}$$

and the activation energy for vacancy migration is

$$E_m = \frac{\partial}{\partial(1/RT)} \ln\left(\frac{1}{\nu_{Cu} + \nu_{Al}}\right) \tag{18}$$

However, the relation between these jump frequencies ν_{Cu} and ν_{Al} and the resulting ordering rate is more complex. Clearly, not every atom jump participates in the ordering. To evaluate the ordering rate, only Cu–Al or Al–Cu jumps will be taken into account. A weighted frequency ν_m^* must be used [66]

$$\frac{1}{\nu_m^*} = \frac{1}{2z\gamma}\left(\frac{1}{\nu_{Cu}} + \frac{1}{\nu_{Al}}\right) \tag{19}$$

where z (= 12) is the coordination number and the value of γ is 1 or 1/7 for directional or short-range order respectively [66]. Then, the activation energy E_m^* associated with ν_m^* is

$$E_m^* = \frac{\partial}{\partial(1/RT)} \ln\left(\frac{1}{\nu_{Cu}} + \frac{1}{\nu_{Al}}\right) \tag{20}$$

As a consequence, while the vacancy lifetime is determined by the faster jump ν_{Al}, the ordering rate is controlled mainly by the slower jump ν_{Cu}, as can be inferred from the results presented below. The frequencies ν_{Cu} and ν_{Al} are related to the diffusion corresponding radioactive tracers by

$$D_{Cu} = \frac{c_V \nu_{Cu} a^2}{1 - \bar{c}} \qquad D_{Al} = \frac{c_V \nu_{Al} a^2}{\bar{c}} \tag{21}$$

where c_V is the vacancy concentration and a the lattice parameter.

In order to compute ν_{Cu} and ν_{Al}, D_{Cu} and D_{Al} were evaluated by the method proposed by Beke et al. [67]. Only available data employing Cu^{64} exist for D_{Cu} in a wide range of Al concentrations [68]. The results obtained for D_{Cu} were in excellent agreement with those data, as can be seen below, which also infers, in principle, that the reliability of the values obtained for D_{Al} is good. The activation energies for tracer diffusion are given by [67]

$$Q_{Cu}(\bar{c}) = \alpha'(\bar{c})\left[T_c(\bar{c}) + \theta\bar{c}(2\bar{c}\ \Delta T - \tilde{T})\right] + \gamma(\bar{c})\left[T_m(Cu) + \bar{c}\tilde{T}\right] \tag{22}$$

$$Q_{Al}(\bar{c}) = \alpha'(\bar{c})\left\{T_c(\bar{c}) + \theta\tilde{T} - \theta\bar{c}\left[2(1-\bar{c})\ \Delta T + \tilde{T}\right]\right\} + \gamma(\bar{c})\left[T_m(Cu) + \tilde{T} + \bar{c}(\tilde{T} - 2\ \Delta T)\right] \tag{23}$$

TABLE 5

Calculation of activation energies for tracer diffusion

Material (at.% Al)	$T_c(\bar{c})$ (K)	$\alpha'(\bar{c})$ ($\times 10^{-3}$ kJ mol^{-1} K^{-1})	$\gamma(\bar{c})$ ($\times 10^{-3}$ kJ mol^{-1} K^{-1})	ΔT (K)	$\tilde{T}$ (K)	Q_{Cu} (kJ mol^{-1})	Q_{Al} (kJ mol^{-1})
19	1313	77.1	72.7	117.2	−94.9	192.6	173.0
13	1323	76.9	72.5	91.2	−120.4	193.5	180.5
6.5	1348	76.7	72.4	48.6	−63.5	195.5	188.0

with

$$T_c(\bar{c}) = T_m(\mathrm{Cu}) + \bar{c}[T_m(\mathrm{Al}) - T_m(\mathrm{Cu})] + 2\bar{c}(1-\bar{c})\,\Delta T \tag{24}$$

where $T_m(\mathrm{Cu})$ and $T_m(\mathrm{Al})$ are the melting temperatures of Cu and Al, $T_c(\bar{c})$ is the mean temperature between the liquidus and solidus and

$$\tilde{T} = \frac{T_m(\mathrm{Al}) - T_m(\mathrm{Cu})}{2} + \Delta T \tag{25}$$

where $\Delta T = W\beta/2\Omega$, β and Ω being constants. It should be noted that if the alloy is in an ideal random state ($W = 0$), $\Delta T = 0$. In eqns. (22) and (23), $\alpha'(\bar{c})$ is a linear interpolated coefficient calculated between $\alpha'(\mathrm{Cu}) = (H_f(\mathrm{Cu})/T_m(\mathrm{Cu}))$ and $\alpha'(\mathrm{Al}) = (H_f(\mathrm{Al})/T_m(\mathrm{Al}))$ where $H_f(\mathrm{Cu})$ and $H_f(\mathrm{Al})$ are the formation energies of vacancies. $\gamma(\bar{c})$ is also a linear interpolated coefficient calculated between $\gamma(\mathrm{Cu})$ and $\gamma(\mathrm{Al})$ obtained from $Q(\mathrm{Cu}) = (\alpha'(\mathrm{Cu}) + \gamma(\mathrm{Cu})T_m(\mathrm{Cu}))$ and $Q(\mathrm{Al}) = (\alpha'(\mathrm{Al}) + \gamma(\mathrm{Al})T_m(\mathrm{Al}))$, $Q(\mathrm{Cu})$ and $Q(\mathrm{Al})$ being the activation energies for self-diffusion. The constant θ is 0.16 [67]. Values for $T_m(\mathrm{Cu})$, $T_m(\mathrm{Al})$ and $T_c(\bar{c})$ were obtain from the equilibrium phase diagram, allowing ΔT to be computed from eqn. (24) and then $\tilde{T}$ from eqn. (25). Values of $H_f(\mathrm{Cu})$ and $H_f(\mathrm{Al})$ were taken from ref. 58. All relevant data and the corresponding values for $Q_{Cu}(\bar{c})$ and $Q_{Al}(\bar{c})$ are listed in Table 5.

It is interesting to note that the activation energies E_2 are lower than the corresponding values for both components. This effect was also observed in some Ag–Au alloys [69] and its explanation is still unclear.

The diffusion constants $D_0(\mathrm{Cu})$ and $D_0(\mathrm{Al})$ were evaluated using [70]

$$\ln\left\{D_0\left[\frac{M(\bar{c})\bar{c}}{RT_c(\bar{c})^2 a^2}\right]^{1/2}\right\} = p\frac{Q(\bar{c})}{T_c(\bar{c})} + \rho \tag{26}$$

where $M(\bar{c})$ is the mass of the "average" CuAl atom and their values were obtained from ref. 34 ($p = 6.64 \times 10^{-2}$ K (kJ mol^{-1})), and $\rho = -4.3$ [70]. The calculations are summarized in Table 6.

TABLE 6

Calculation of tracer diffusion constants

Material (at.% Al)	$M(\bar{c})$ (10^{-26} kg at^{-1})	a ($\times 10^{-10}$ m)	$D_{0(Cu)}$ ($\times 10^{-4}$ m^2 s^{-1})	$D_{0(Al)}$ ($\times 10^{-5}$ m^2 s^{-1})
19	9.40	3.69	1.16	5.18
13	9.73	3.67	1.34	9.85
6.5	10.2	3.64	1.69	7.38

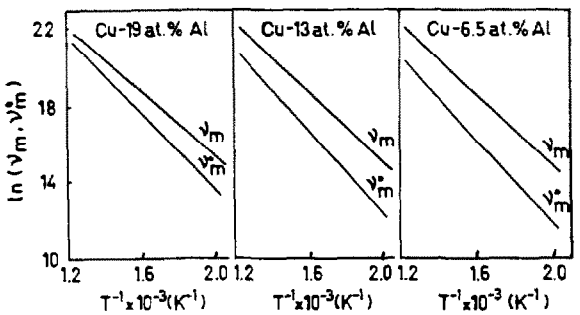

Fig. 10. Vacancy jump frequency to sinks (ν_m) and vacancy jump frequency controlling the short-range ordering rate (ν_m^*) plotted against the reciprocal of temperature for αCu–Al alloys.

With the values of Q_{Cu}, Q_{Al}, $D_{0(Cu)}$ and $D_{0(Al)}$ and noting that

$$\nu_m = \nu_{0m} \exp(-E_m/RT) \quad \text{and} \quad \nu_m^* = \nu_{0m}^* \exp(-E_m^*/RT) \tag{27}$$

and because an Arrhenius plot is obeyed, values for ν_{0m}, ν_{0m}^*, E_m and E_m^* can be calculated from eqns. (17)–(21) using Fig. 10. This plot was made in the temperature range below the melting temperature of Al. The results are listed in Table 7.

Computed values for ν_{0m} and ν_{0m}^* are in excellent agreement with those obtained for other alloy systems [53,71], as are the activation energies for vacancy migration to sinks E_m [61]. Values for E_m^* are larger but still smaller than those obtained from the thermograms for E_1 which determine

TABLE 7

Values for activation energies for vacancy migration and jump frequency constants

Material (at.% Al)	E_m (kJ mol^{-1})	E_m^* (kJ mol^{-1})	ν_{0m} ($\times 10^{14}$ s^{-1})	ν_{0m}^* ($\times 10^{14}$ s^{-1})
19	70.4	82.0	1.02	3.14
13	74.2	86.7	2.0	3.16
6.5	77.1	89.6	3.5	3.7

the ordering rate. E_m and E_m^* correspond to monovacancies and, in the absence of bounded vacancies the effective activation energies E_1 would be expected to be very close to E_m^* for each alloy concentration. However, it has been shown here that the influence of vacancy complexes with lower mobility may contribute to increases in E_1 and then it is expected to be larger than E_m^*. Therefore, it follows consistently that $E_1 > E_m^* > E_m$, as calculated.

The connection between the kinetic path of stage 1 given by y_1 and the relief of the vacancy supersaturation $S = (c_v - c_{ve})/(c_v(0) - c_{ve})$, where $c_v(0)$ is the vacancy concentration after the quench, c_{ve} is the equilibrium concentration and c_v the actual vacancy concentration at temperature T, will now be investigated. First-order kinetics were assumed for the elimination of vacancy supersaturation, which assumes that elimination takes place on fixed sinks [54]. The characteristic process frequency factor is given by $k_{0m} = \rho_v \nu_{0m}$, where ρ_v is the effective sink density. For a dislocation density $\delta = 10^7$ cm cm^{-3}, as expected in the present material and using the conventional relation $\rho_v = 2\pi b\delta/\ln(r_s/r_c)$ in which r_s is the average distance between dislocations, r_c the capture radius of the dislocation and b the atom jump distance, $\rho_v = 4.3 \times 10^{-8}$ at^{-1} is obtained. This value, in conjunction with the values calculated for ν_{0m}, gives $k_{0m} = 6.7 \times 10^5$, 1.3×10^6 and 2.3×10^6 s^{-1} for 19, 13 and 6.5% Al. Furthermore, under non-isothermal conditions, $S = \exp(-k_{0m}\theta_1(E_m))$. Curves for S and y_1 plotted against T are shown in Fig. 11. For illustration purposes only, an S curve was plotted for a deformed material with $\delta = 10^{11}$ cm cm^{-3}, which

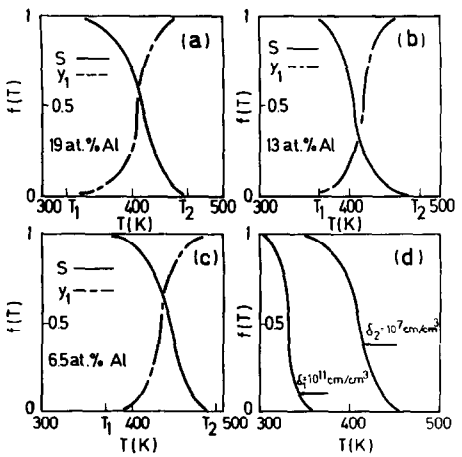

Fig. 11. Kinetics of the supersaturation vacancy decay (S) for αCu–Al alloys quenched from 873 K. The reacted fraction during stage 1 (y_1) is also shown for each alloy. In Fig. 11(d), the supersaturation decay is plotted for Cu–19 at.% Al, showing two different dislocation densities representative of deformed (δ_1) and annealed (δ_2) materials; $\phi = 0.33$ K s^{-1}.

corresponds to $\rho_v = 10^{-5}$ at^{-1}. For such a specimen, it can be inferred that stage 1 should go to completion at a lower temperature. Comparison of both y_1 and S curves, confirms that stage 1 effectively corresponds to an SRO process assisted by excess vacancies, because in all cases it goes to completion just when the vacancy supersaturation vanishes. Moreover, both curves exhibit symmetrical kinetic paths. It is then inferred necessarily that during stage 2 the ordering process must be completed, assisted by equilibrium vacancies and by vacancy complexes which were not yet eliminated during stage 1. This behaviour is consistent with the determined values for k_{02} from the thermogram of Fig. 1. In fact, one can calculate for an SRO process assisted by equilibrium vacancies only, a process frequency factor

$$k_{02}^* = \eta A \nu_{0m}^* \tag{28}$$

where $A = \exp(\Delta S_f/R) \simeq 2$, ΔS_f being the formation entropy of a vacancy, with η and efficiency factor of order unity, as generally used [72]. Thus, $k_{02}^* = 6.3 \times 10^{14}$, 7.7×10^{14} and 7.4×10^{14} s^{-1} for 19, 13 and 6.5% Al, in fairly good agreement with the values of k_{02} listed in Table 3. Values of k_{01}^* can also be roughly estimated. The initial and final values for k_{01}^* are $k_{01i}^* = \eta c_v(0) \nu_{0m}^*$ at T_1 and $k_{01f} = \eta c_{veq} \nu_{0m}^*$ at T_2 when stage 1 goes to completion, because the initial excess vacancy concentration falls as the temperature is raised, $c_v(0)$ being much higher than c_{veq} at T_2. For simplicity, it will be assumed that k_{01}^* calculated by non-isothermal techniques is the average of the initial and final values. Hence

$$k_{01}^* = \frac{\eta c_v(0) \nu_{0m}^*}{2} \tag{29}$$

neglecting k_{01f}^* with respect to k_{01}. With the values of the effective energy for vacancy formation $E_f = E_2 - E_1$, and considering as a first approximation that $c_v(0) = A^* \exp(-E_f/RT_q)$, one obtains $c_v(0) = 4.6 \times 10^{-4}$, 1.6×10^{-4} and 5.2×10^{-5} for 19, 13 and 6.5% Al, giving $k_{01}^* = 7 \times 10^{10}$, 3.1×10^{10} and 1×10^{10} s^{-1} if $\eta \simeq 1$. Although the agreement with the values calculated from the DSC traces is very good for Cu–19% Al and Cu–13% Al, for Cu–6.5% Al it is poorer, presumably because different efficiency factors should be considered for different Al contents.

The method of Beke and co-workers [67,70] used to compute tracer diffusion coefficients, also allows an estimation of the binding energy of divacancies, which can be expressed by

$$E_{2v}(\bar{c}) = \theta \alpha'(\bar{c}) T_c(\bar{c}) \tag{30}$$

Using the computed data for θ, $\alpha'(\bar{c})$ and $T_c(\bar{c})$, $E_{2v} = 16.2$, 16.3 and 16.6 kJ mol^{-1} for 19, 13 and 6.5% Al. Therefore, it is advisable, in the absence of reported data, to take the average value of $E_{2v} = 16.4$ kJ mol^{-1} (0.17 eV).

When the fractional concentration of solute atoms is higher than that of

vacancies and the binding energy E_{2v} of a divacancy (16.4 kJ mol^{-1}) is smaller than the binding energy E_{vs} of a single vacancy to a solute atom (21.8 kJ mol^{-1}), then the formation of divacancies can be ignored because a single vacancy has more chance of encountering a solute atom than another vacancy. It was assumed that this is the case for αCu–Al alloys in the present work.

Concentration dependence of the relative increase of the SRO parameter

The fractional increase in α during a DSC experiment depends on many factors, which make the above treatment somewhat simplified. As the alloy composition increases in quenched alloys, the excess vacancy concentration, the vacancy mobility, the bound-to-free vacancy ratio and the degree of SRO also increase during stage 1. But the increase in SRO degree produces a decrease in the vacancy concentration and a decrease in the vacancy mobility. Also the bound-to-free vacancy ratio is expected to become lower. Therefore, the net free vacancy concentration and the effective vacancy mobility are strongly dependent on the interplay of all these factors during stage 1. They are shown schematically in Fig. 12. The controlling factors for the same material variables during stage 2 are also shown on the figure.

On the basis of this flow chart, the fractional increase of the first SRO parameter $R_1 = (\alpha_{E_2} - \alpha_{E_1})/\alpha_{E_1}$ during stage 1 is now considered. As discussed above, there is simultaneous interplay of some effects in favour and of others in opposition to a net relative increase in the first SRO parameter. It is then plausible that R_1 goes through an extreme value for intermediate Al contents. In fact, a maximum is observed for Cu–13% Al, as shown in Fig. 13. In the same figure it can be seen that the fractional increase of the first SRO parameter, $R_2 = (\alpha_{T_2} - \alpha_{E_2})/\alpha_{E_2}$, corresponding to stage 2, decreases systematically as the alloy becomes more concentrated. If the same arguments are valid for stage 2, the observed tendency indicates that the factors retarding the net relative increment in R_2 become much stronger than in stage 1 with increasing aluminium content. This behaviour is not unexpected because in stage 2, where the degree of SRO is larger than in stage 1, both the free vacancy mobility and the vacancy concentration reducing effects would be consequently more conspicuous. Thus, extreme values of R_2 might not be present over the whole range of alloy compositions, as was effectively observed.

CONCLUSIONS

The investigation by differential scanning calorimetry of the ordering process in αCu–Al alloys leads to the following conclusions:

(a) Rising temperature experiments are better interpreted in terms of a

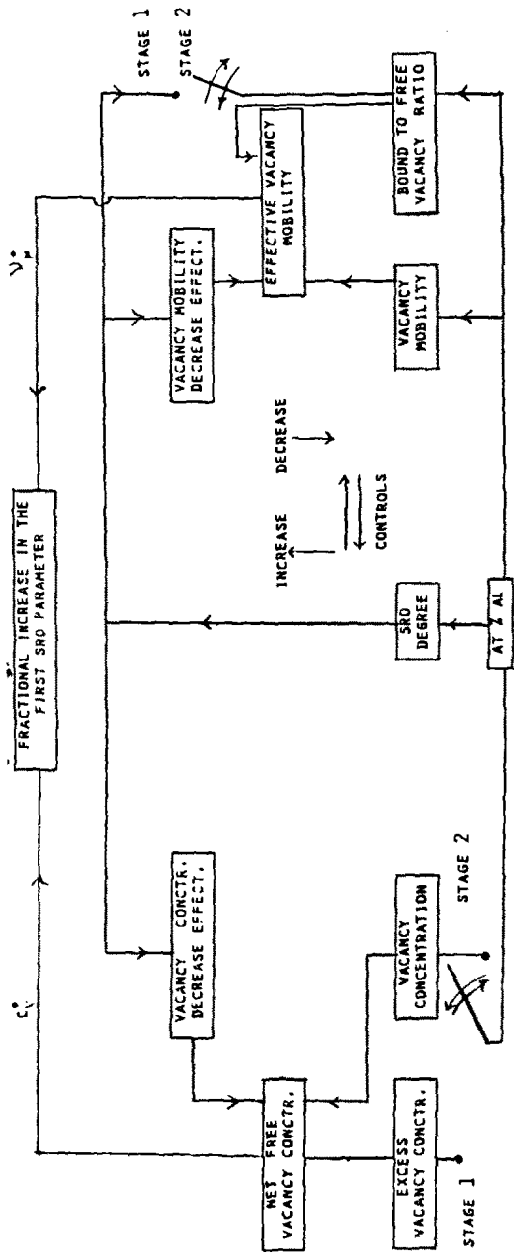

Fig. 12. Flow chart illustrating the controlling factors which determine the fractional increase in the first SRO parameter: c_v^*, effective vacancy concentration; ν_m^*, effective vacancy mobility.

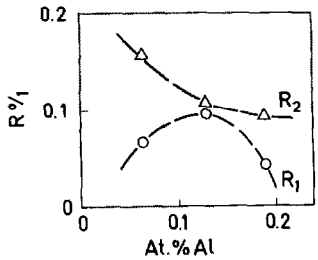

Fig. 13. Fractional increase of the first SRO parameter for stages 1 (R_1) and 2 (R_2) as a function of aluminium content.

homogeneous SRO rather than a heterogeneous DO model. This feature is also supported by electron diffraction observations.

(b) Under non-isothermal heating after quenching as described above, SRO takes place in two stages, stage 1 at lower temperatures and stage 2 at higher temperatures. The SRO kinetics until equilibrium is attained become faster as the aluminium content increases. Stage 1 ordering is assisted by the migration of excess vacancies, while stage 2 ordering is assisted by the migration of equilibrium vacancies.

(c) The concentration of excess vacancies is mainly controlled by the quenching temperature, the shape of the sample being quenched, the quenching rate and the number of vacancy sinks. These factors, in turn, control the predominance of each stage.

(d) An expression which describes the overall SRO kinetics for both stages 1 and 2 was developed. The kinetic process can also be evaluated in terms of the first SRO parameter, making use of a method suitable for obtaining boundary values. In furnace-cooled alloys, only stage 3 is observed.

(e) Effective activation energies for stage 1 are consistent with those for vacancy migration controlling the ordering rate, while activation energies for stage 2 are consistent with those for interdiffusion. Activation energies for vacancy migration controlling their lifetime resulted in smaller values.

(f) The number of less mobile vacancy–solute complexes may be important in these alloys. They are likely to be annihilated at temperatures in the range of stage 2. A solute–vacancy binding energy of 21.8 kJ mol^{-1} and a divacancy binding energy of 16.4 kJ mol^{-1} were estimated.

(g) Process frequency factor values are in agreement with those expected from the development of SRO during stages 1 and 2.

(h) The fractional increase of short-range order during stages 1 and 2 in quenched alloys is a complex interplay of vacancy concentration and vacancy mobility effects which can be understood using a flow diagram.

ACKNOWLEDGEMENTS

The author expresses sincere thanks to Professor Jaroslav Šesták for many valuable suggestions. He also thanks the investigator Eduardo Donoso for his important contribution to this research work. This work was supported by the Fondo Nacional de Desarrollo Científico y Tecnológico (FONDECYT) Project No. 92-0891 and the Instituto de Investigaciones y Ensayes de Materiales, Faculted de Ciencias Físicas y Matemáticas, Universidad de Chile.

REFERENCES

1 M.S. Wechsler and R.H. Kernohan, J. Phys. Chem. Solids, 7 (1958) 307.
2 S. Matsuo and L.M. Clarebrough, Acta Metall., 11 (1963) 1195.
3 B. Borie and C.J. Sparks, Jr., Acta Crystallogr., 17 (1964) 827.
4 V.Y. Panin, V.P. Fadin and L.D. Kuznetsova, Fiz. Met. Metalloved., 19 (1965) 316.
5 V.I. Iveronova, A.A. Katnslelson and G.P. Revkevich, Fiz. Met. Metalloved., 26 (1968) 106.
6 R.O. Scattergood, S.C. Moss and M.B. Bever, Acta Metall., 18 (1970) 1087.
7 N. Kuwano, Y. Tomokiyo, C. Kinoshita and T. Eguchi, Trans. Jpn. Inst. Met., 15 (1974) 338.
8 Y. Kitano and Y. Kimura, J. Phys. Soc. Jpn., 32 (1972) 1430.
9 J.E. Epperson, P. Furnrohr and C. Ortiz, Acta Crystallogr., A34 (1978) 667.
10 R.W. Cahn and R.G. Davies, Philos. Mag., 5 (1960) 1119.
11 W. Gaudig and H. Warlimong, Z. Metallkd., 60 (1969) 488.
12 Y. Tomokiyo, N. Kuwano and T. Eguchi, J. Phys. Soc. Jpn., 35 (1973) 618.
13 Y. Tomokiyo, K. Kabu and T. Eguchi, Jpn. Inst. Met., 15 (1974) 39.
14 A. Varschavsky, M.I. Pérez and T. Löbel, Metall. Trans., 6A (1975) 577.
15 W. Gaudig and H. Warlimont, Acta Metall., 26 (1978) 709.
16 J.M. Popplewell and J. Crane, Metall. Trans., 2 (1971) 341.
17 C. Kinoshita, Y. Tomokiyo, H. Matsuda and T. Eguchi, Trans. Jpn. Inst. Met., 14 (1973) 91.
18 M. Zehetbauer, L. Trieb and H.P. Aubauer, Z. Metallkd., 67 (1976) 431.
19 A. Varschavsky, Mater. Sci. Eng., 22 (1976) 141.
20 A. Varschavsky and E. Donoso, Mater. Sci. Eng., 32 (1978) 65.
21 E. Donoso and A. Varschavsky, Mater. Sci. Eng., 37 (1979) 151.
22 A. Varschavsky and E. Donoso, Mater. Sci. Eng., 40 (1979) 119.
23 A. Varschavsky and E. Donoso, Mater. Sci. Eng. A, 10 (1988) 231.
24 A. Varschavsky and E. Donoso, Mater. Sci. Eng. A, 104 (1988) 141.
25 G. Veith, L. Trieb, W. Puschl and H.P. Aubauer, Phys. Status Solidi, 27 (1975) 59; Scr. Metall., 9 (1975) 737.
26 A. Varschavsky and E. Donoso, Thermochim. Acta, 69 (1983) 341.
27 M.J.S. Wechsler and R.H. Kernohan, Acta Metall., 7 (1959) 599.
28 L. Trieb and G. Veith, Acta Metall., 26 (1978) 185.
29 C.R. Brooks and E.E. Stansbury, Acta Metall., 11 (1963) 1303.
30 Y. Tomokiyo, N. Kuwano and T. Eguchi, Trans. Jpn. Inst. Met., 26 (1975) 489.
31 A. Varschavsky, Metall. Trans., 13A (1982) 801.
32 A. Varschavsky and E. Donoso, Metall. Trans., 14A (1983) 875.
33 A. Varschavsky and E. Donoso, Metall. Trans., 15A (1984) 1999.
34 A. Varschavsky and E. Donoso, J. Mater. Sci., 21 (1986) 3873.

35 W. Pfeiler and R. Reihsner, Phys. Status Solidi (a), 97 (1986) 377.
36 A. Varschavsky and E. Donoso, Mater. Sci. Eng., (in press).
37 N. Kuwano, I. Ogata and T. Eguchi, Trans. Jpn. Inst. Met., 18 (1977) 87.
38 J.M. Roland, X. Quillard and A. Moreau, Phys. Stat. Solid. A, 64 (1981) 45.
39 A. Varschavsky, J. Mater. Sci., 26 (1991) 3603.
40 K. Mitsui, Y. Mishima and T. Suzuki, Philos. Mag., 59A (1989) 123.
41 K. Mitsui, Y. Mishima and T. Suzuki, Philos. Mag., 53A (1986) 357.
42 K. Mitsui, Philos. Mag., 53A (1986) 447.
43 H.P. Aubauer, Acta Metall., 20 (1972) 165.
44 H.E. Kissinger, Anal. Chem., 28 (1957) 1702.
45 C.Y. Li and A.S. Novick, Phys. Rev., 103 (1956) 294.
46 A.C. Novick, Phys. Rev., 88 (1952) 925.
47 L. Trieb, K. Siebinger and H.P. Aubauer, Scr. Metall., 31 (1973) 245.
48 K.N. Ninan, J. Therm. Anal., 35 (1989) 1267.
49 C. Sandu and R. Singh, Thermochim. Acta, 159 (1990) 267.
50 J. Šesták, J. Therm. Anal., 33 (1988) 1263.
51 J. Šesták, J. Therm. Anal., 36 (1990) 1997.
52 J. Málek, J. Šesták, F. Rouquerol, J. Rouquerol, J.M. Criado and A. Ortega, J. Therm. Anal. (in press).
53 W. Kohl, R. Scheffel, H. Heidsiek and K. Lucke, Acta Metall., 31 (1983) 1895.
54 W. Pfeiler, Acta Metall., 36 (1988) 2417.
55 S. Radelaar, J. Phys. Chem. Solids, 31 (1970) 219.
56 W. Pfeiler and R. Reihsner, Phys. Status Solidi, (1) 97 (1986) 375.
57 A.K. Mukhopadhyay, G.J. Shiflet and E.A. Starke, Scr. Metall. Mater., 24 (1990) 307.
58 H. Kimura and R. Maddin, Quench Hardening in Metals, North-Holland, Amsterdam, 1971, p. 17.
59 J.I. Takamura, M. Doyama and H. Kisitani, Point Defects and Defect Interactions in Metals, Univ. of Tokyo Press, North-Holland, Amsterdam, 1982, p. 452.
60 S. Ozbilen and H.M. Flower, Acta Metall., 37 (1989) 2993.
61 V.P. Fadin and V.Ye Panin, Fiz. Met. Metalloved., 14 (1962) 517.
62 F.W. Schapink, Philos. Mag., 12 (1965) 1055.
63 G. Bérces and I. Kovács, Philos. Mag., 48A (1983) 883.
64 P.V. Petrenko and A.A. Tatarov, Phys. Met. Metall., 56 (1983) 80.
65 K.K. Mansur, Acta Metall., 29 (1981) 375.
66 A. Caplain and W. Chambron, Acta Metall., 25 (1977) 1001.
67 D.L. Beke, I. Godény, F.J. Kedves and G. Erdélyi, J. Phys. Chem. Solids, 40 (1979) 543.
68 J. Kucera and B. Million, Metall. Trans., 1 (1970) 2599.
69 S. Radelaar, Phys. Status Solidi, 27 (1968) K 63.
70 D.L. Beke, I. Uzonyi and F.J. Kedves, Philos. Mag., 44 (1981) 983.
71 M. Halbwachs and J. Hillairet, Phys. Rev. B, 18 (1978) 4927.
72 E. Balanzat and J. Hillairet, J. Phys. F. Metal. Phys., 11 (1981) 1977.